Structure of flux tubes in SU(2)

A. M. Green*

Research Institute for Theoretical Physics, University of Helsinki, Finland

C. Michael[†]

Theoretical Physics Division, Department of Mathematical Sciences, University of Liverpool, Liverpool, United Kingdom

P. S. Spencer[‡]

Research Institute for Theoretical Physics, University of Helsinki, Finland

The spatial distribution of the action and energy in the color fields of flux tubes is studied in lattice SU(2) field theory for static quarks at separations up to 1 fm. Special attention is paid to the structure of the color fields associated with an excited flux tube with E_u symmetry. We compare our results with hadronic string and flux-tube models. Sum rules are used to extract generalized β functions, to describe the expected color field behavior, and to cross-check the methods used. [S0556-2821(97)02903-2]

I. INTRODUCTION

Confinement in QCD is a nonperturbative phenomenon and lattice gauge theory techniques are well suited to its study. One of the simplest manifestations of confinement in pure glue QCD is the potential energy $V(R)$ between static quarks at separation R which increases with R. To investigate this in detail, it is possible to probe the spatial distribution of the color fields around such static quarks. This exploration of the nature of the flux between static quarks has a long history. Typical points of interest are the transverse extent of the flux tube and the nature of the color fields (i.e., electric or magnetic). A hadronic string approach gives a reasonable description of the interquark potential at large separation. Here we explore this further by investigating the distribution of color fields for gluonic excitations of this potential and comparing our results with models for the flux tube in this case also.

On a lattice the technique to explore the color field distributions is to measure the correlation of a plaquette □ [here defined as $\square=\frac{1}{2}\mathrm{Tr}(1-U_\square)$] with the generalized Wilson loop $W(R,T)$ that creates the static quark-antiquark at separation R. See Fig. 1 for an illustration. Locating the plaquette at $t=T/2$, in the limit $T\to\infty$ the following expression isolates the contribution from the color field at position $\mathbf{r}$ from the plaquette oriented in the μ,ν plane:

$$f_R^{\mu\nu}(\mathbf{r})=\left[\frac{\langle W(R,T)\square_{\mathbf{r}}^{\mu\nu}\rangle-\langle W(R,T)\rangle\langle\square^{\mu\nu}\rangle}{\langle W(R,T)\rangle}\right]. \quad (1)$$

These contributions are related in the naive continuum limit to the mean squared fluctuation of the Minkowski color fields by

*Electronic address: green@phcu.helsinki.fi

[†]Electronic address: cmi@liv.ac.uk

[‡]Electronic address: paddy.spencer@parallax.co.uk; Current address: Parallax Solutions Ltd., Stonecourt, Siskin Drive, Coventry CV3 4FJ, United Kingdom.

$$f_R^{ij}(\mathbf{r})\to\frac{a^4}{\beta}B_k^2(\mathbf{r}) \quad \text{with} \quad i,j,k \quad \text{cyclic}$$

and

$$f_R^{i4}(\mathbf{r})\to-\frac{a^4}{\beta}E_i^2(\mathbf{r}). \quad (2)$$

We shall wish to distinguish electric and magnetic color fields with different orientations with respect to the interquark separation axis (longitudinal—taken as one-axis) and adopt the notation that

$$\mathcal{E}_L=f^{41}, \quad \mathcal{E}_T=f^{42,43}, \quad \mathcal{B}_T=f^{12,13}, \quad \mathcal{B}_L=f^{23,32}. \quad (3)$$

It will be convenient to discuss combinations corresponding naively to the action (S) and energy (E) densities of the gluon field. These are given by

$$S(\mathbf{r})=-(\mathcal{E}_L+2\mathcal{E}_T+2\mathcal{B}_T+\mathcal{B}_L) \quad (4)$$

and

$$E(\mathbf{r})=E_L(\mathbf{r})+2E_T(\mathbf{r})=-(\mathcal{E}_L-\mathcal{B}_L)-2(\mathcal{E}_T-\mathcal{B}_T). \quad (5)$$
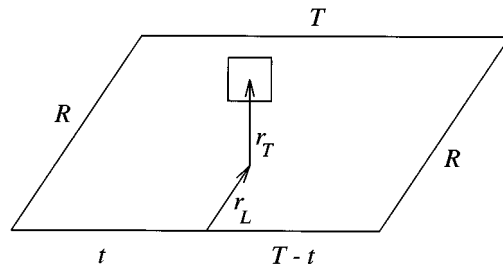

FIG. 1. The generalized Wilson loop of size $R\times T$ with the plaquette located at time t, longitudinal coordinate r_L, and transverse coordinate r_T.

Note that since the color field contributions come from a cancellation between the value in a static potential and that in the vacuum, either sign is possible.

The color field distributions are quite difficult to measure on a lattice because the correlation of Eq. (1) involves delicate cancellations. Recent results [1] and [2] have concentrated on the simpler case of SU(2) color in order to achieve sufficient statistical accuracy. It is expected that the salient features of confinement in SU(2) are very similar to those in the realistic case of SU(3). Here we focus our attention on the color field distributions at $\beta = 2.4$ for which the lattice spacing $a \approx 0.1$ fm should be sufficiently small for our purposes. The action and energy densities are measured on a lattice by using plaquettes of area a^2, and hence, do not have a continuum limit as $a \rightarrow 0$. To achieve a continuum limit would require to measure energy and action by using loops of fixed physical size rather than plaquettes. In the following, we quote our results in lattice units with the normalization as given above in Eq. (1).

Different strategies have been used to improve the signal to noise in the lattice determination of the color fields. Here we focus on one method, as described in Sec. III, which is to create operators which produce ground state potentials with very little contamination of excited states. As described in the next section, we are able to achieve this using fuzzed links and a variational approach. Because we wish to study sum rules which involve sums over all spatial positions, we do not employ multihit techniques such as those used in Ref. [1]. We do not use, either, the proposal of Ref. [2] to treat $\langle \Box^{\mu\nu} \rangle$ in Eq. (1) as a quasilocal average of the plaquette in the correlation since, although it reduces the noise, it also modifies the signal.

Lattice sum rules have been derived [3–5] which relate the sum over all space of the plaquette correlation to expressions involving the potential $V(R)$ and generalized β functions. These sum rules have been used in an attempt to extract such β functions [6,7]. Here we consider a larger set of sum rules and we make a careful evaluation of these sum rules to extract the generalized β functions and to validate our methods. This is described in Sec. IV. A preliminary account has been given in Ref. [8].

We present our results for the spatial distributions of the color fields in Sec. V. One feature that goes beyond previous work, is that we also measure the color field distribution in the lowest lying gluonic excitation of the static quark potential. This lowest gluonic excitation has nonzero angular momentum about the interquark axis and plays a role in hybrid meson spectroscopy. Hadronic string models predict such excited modes and agreement with the energy levels determined on a lattice has been found [9,10]. Here we are able to explore the spatial distribution of this excited gluonic mode to make more detailed comparisons with models. We have also explored a higher gluonic excited state: the first excited state with the symmetry of the ground state. In this case we have been unable to extract unambiguously the color fields associated with this state so we do not report on it further here.

II. OPERATORS FOR STATIC POTENTIALS

To explore the color field distributions around static quarks at separation R, we need to find efficient lattice operators to create such states. Efficient here means having a small contamination of excited states while still allowing a good signal to noise for correlations of interest. We build on the experience of studying the corresponding potentials [9] and use an iterative fuzzing prescription to create the spatial paths P_i of length R, where different levels of iteration of fuzzing are represented by i. In detail, we use a number of recursive iterations of replacing each spatial link by the projected sum of (4 × straight link + 4 spatial U bends) and then multiply these fuzzed links to make the spatial path needed. The correlation of spatial path P_i at time t and P_j at time $t + T$ then gives the generalized Wilson loop $W_{ij}(T)$ — see Fig. 1. We use a $16^3 \times 32$ lattice at $\beta = 2.4$ for this study with the SU(2) gauge group. For many purposes SU(2) color provides an excellent test bed for QCD studies. In this work the scale as set by the string tension corresponds to a lattice spacing $a \approx 0.6$ GeV$^{-1} \approx 0.12$ fm. The data sample used comes from a comprehensive study of 80 blocks (60 blocks for $R \leq 3$) of 125 measurements separated by four update sweeps (three over-relaxation plus one heatbath). Error estimates use a full bootstrap analysis of these blocks.

The fuzzed link operator P_i to create a static quark and antiquark at separation R with a color field in a state of a given lattice symmetry will have an expansion in terms of the eigenstates of the transfer matrix,

$$|R\rangle = c_0 |V_0\rangle + c_1 |V_1\rangle + \cdots,\qquad(6)$$

with the measured correlation of a generalized Wilson loop given by

$$W(R,T) = \langle R_0 | R_T \rangle = c_0^2 e^{-V_0 T}(1 + h^2 + \cdots),\qquad(7)$$

where

$$h = \frac{c_1}{c_0} e^{-(V_1 - V_0)T/2}.\qquad(8)$$

We shall see that the contamination by excited states needs to be minimized so that $h \ll 1$, while, in order to retain a reasonable signal to noise, we should like to achieve this with $T = 2$. In order to calibrate the contamination by excited states we show in Table I the results for the effective potential defined as

$$V_{\text{eff}}(R,T) = -\ln[W(R,T)/W(R,T-1)].\qquad(9)$$

We measure the generalized correlation to $T = 4$ for $R > 3$ and to $T = 6$ for $R \leq 3$. The signal is too noisy at larger T values to be a useful guide. We use a variational method

TABLE I. Potential energy values for the symmetric A_{1g} case.

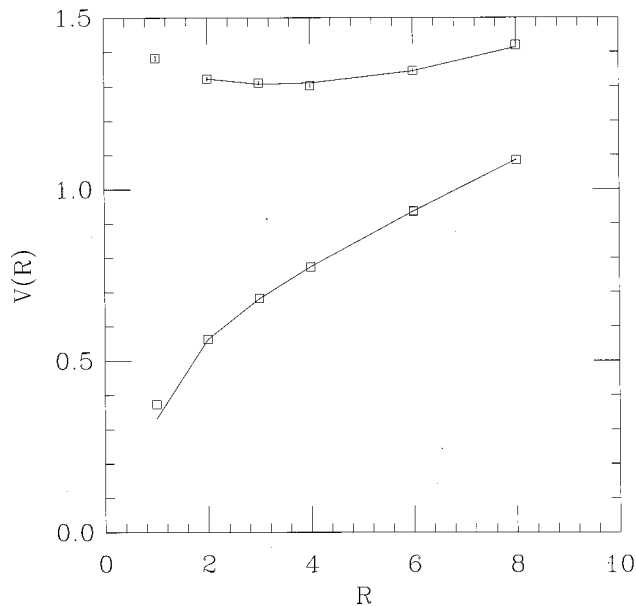| R	Fuzz levels	V_{eff} T 3:2	V_{eff} T 4:3	V_{eff} $T \rightarrow \infty$	$|h|$
1	2,13	0.37333(5)	0.37326(5)	0.37325(5)	0.010
2	2,13	0.56280(14)	0.56247(17)	0.56234(18)	0.026
3	2,13	0.68233(24)	0.68131(32)	0.68088(36)	0.046
4	0,16,40	0.77512(24)	0.77394(34)	0.77329(42)	0.053
6	0,16,40	0.93844(51)	0.93685(80)	0.93585(103)	0.065
8	0,16,40	1.09154(77)	1.08801(131)	1.08558(180)	0.100

FIG. 2. The energies of the potentials in lattice units for separation R with an interpolation from Eqs. (15) and (16). The data points are for the symmetric ground state (A_{1g} representation) and first gluonic excitation (E_u representation).

with a combination of paths with different fuzzing levels chosen so that the effective potential is minimized for $T=1$. This combination is then used at all T and gives the effective potential values shown in Table I. As an estimate of the true ground state potential energy one could use the $T=4$ effective potential, however, this is an upper limit because of excited state contributions. Another estimate can be made by assuming [11] that the change in effective energy from $T=3$ to 4, namely $\Delta V = V_{eff}(3:2) - V_{eff}(4:3)$, is given entirely by the contribution of one excited state with an energy difference $V_1 - V_0$ determined by the variational analysis outlined above. Defining $\lambda = e^{-(V_1-V_0)}$, this extrapolated estimate will lie below $V_{eff}(3:2)$ by $\Delta E/(1-\lambda)$ and this value is shown in Table I labeled as $T \to \infty$. The difference between these two methods to extract the ground state potential energy gives an estimate of the systematic error from extrapolation in T. The potentials are the data points plotted in Fig. 2.

In order to estimate the magnitude of the excited state contamination in the state for $T=2$, we use the same approximation of one excited state only for $T>2$. Then one has that $h^2 \approx \Delta E/(1-\lambda)^2$. The values of h shown in the Tables are for $T=2$ which corresponds to our operator having contamination h at $t=T/2=1$, namely one time step away. We see that for the symmetric (A_{1g}) representation, the contamination h is quite small.

We also study potentials between static quarks with gluonic excitations in the E_u representation. For this case [12] we need U shaped paths (actually the combination $\sqcap - \sqcup$ with the extension in the transverse spatial direction). For this representation, we also need to extract the ground state, and results from generalized Wilson loops are given in Table II. Here we have used a single fuzzing level, but two different values of the transverse extent d of the U-shaped paths.

TABLE II. Potential energy values for the gluonic excitation with E_u symmetry.

R	Fuzz level	d	V_{eff} T 3:2	V_{eff} T 4:3	V_{eff} $T \to \infty$	$|h|$
1	13	1, 2	1.4102(12)	1.3955(33)	1.3813(65)	0.24
2	13	1, 2	1.3484(11)	1.3346(25)	1.3218(49)	0.23
3	13	1, 2	1.3237(11)	1.3164(25)	1.3099(43)	0.16
4	16	1, 4	1.3157(9)	1.3094(20)	1.3018(41)	0.17
6	16	1, 4	1.3569(9)	1.3519(21)	1.3455(44)	0.16
8	16	1, 4	1.4341(11)	1.4282(27)	1.4200(62)	0.18

As shown, the excited state contaminations are significantly higher for this representation than for the symmetric A_{1g} case.

III. LATTICE EVALUATION OF THE COLOR FIELDS

To study the color fields in the ground state of the static quark-antiquark at separation R, we need to evaluate the difference of the expectation value of a plaquette in that ground state with its value in the vacuum:

$$f_R(\mathbf{r}) = \frac{\langle V_0 | \Box_{\mathbf{r}} | V_0 \rangle}{\langle V_0 | V_0 \rangle} - \langle 0 | \Box | 0 \rangle. \qquad (10)$$

This quantity is to be extracted from lattice observables using the geometry shown in Fig. 1. In terms of the decomposition of our operators into eigenstates of the transfer matrix, the measured matrix element of a plaquette at t in the generalized Wilson loop of size $R \times T$ is given by

$$\langle R_0 | \Box_t | R_T \rangle = c_0^2 e^{-V_0 T} \Big(\langle V_0 | \Box | V_0 \rangle + \frac{c_1}{c_0}$$
$$\times [e^{-(V_1-V_0)t} + e^{-(V_1-V_0)(T-t)}]$$
$$\times \langle V_1 | \Box | V_0 \rangle + \cdots \Big). \qquad (11)$$

This clearly highlights the central problem which is that contributions from excited state contaminations will be much larger here than for the determination of the total potential energy because of the presence of off diagonal terms (e.g., $\langle V_1 | \Box | V_0 \rangle$). In order to extract the required quantity $\langle V_0 | \Box | V_0 \rangle$, we need to minimize the excited state contributions by taking $T-t \geq 1$ and $t \geq 1$ as discussed in the previous section. For the case when $T=2$ and $t=1$, the excited state contribution will have a coefficient given by $2h$ with h evaluated at $T=2$—as estimated in Tables I and II. For example, to reduce the excited state contamination to $\lesssim 10\%$, one needs $|h| < 0.05$. The electric plaquettes are extended by one unit in the time direction, however, so one needs $T=3$ to ensure a separation of at least one unit to obtain a sufficiently pure ground state. We are also able to investigate the excited state contamination directly by measuring the plaquette correlation for $T > 3$.

For odd T values, we evaluate the electric plaquette with center at $t = T/2$ and average the magnetic plaquettes over
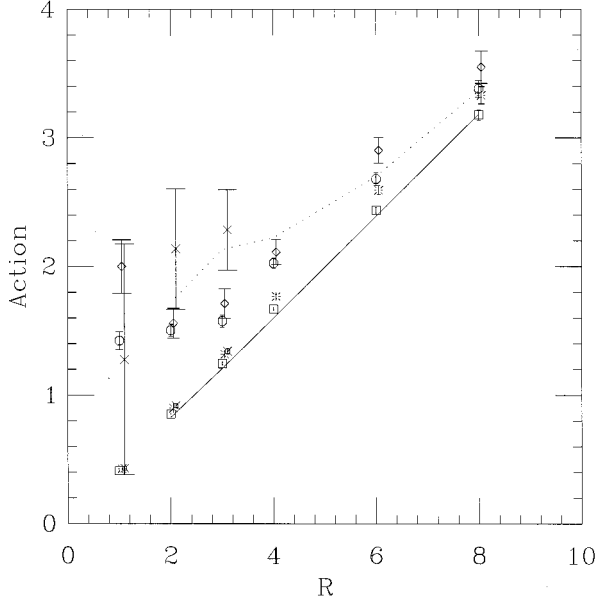
FIG. 3. The color flux contributions in lattice units for separation R corresponding to the action (S) sum rule of Eq. (12) for the static quark potential. The expressions for the left-hand sides derived from the measured potentials as discussed in the text are shown by the lines. The data points for the symmetric ground state (A_{1g} representation) are shown by squares ($T=3$), bursts ($T=4$), and fancy squares ($T=5$). For the transverse gluonic excitation (E_u representation), the data are shown by octagons ($T=3$), diamonds ($T=4$), and crosses ($T=5$).

$t=(T\pm1)/2$. For even T, we average the electric plaquettes over positions with center at $t=(T\pm1)/2$ whereas the magnetic plaquettes are at $t=T/2$.

For the sum rule study, we need the sum of plaquettes over all space in principle. On the lattice, we sum the plaquettes over all transverse space (a 16×16 plane) for each r_L. The sum over r_L is then approximated by selecting the region within ±2 lattice units of the Wilson loop (i.e., from $r_L=-2$ to $R+2$). We checked that this approximation did not introduce any significant error since the missing r_L region contributes noise and no signal to the correlation. Because we sum all plaquettes including those adjacent to the generalized Wilson loop, it is not appropriate to use variance reducing techniques such as multihit.

For our study at the center point between the static quarks, $r_L=R/2$, we average the plaquettes with a corner (or side) at each value of the transverse distance r_T along a lattice axis.

IV. SUM RULES FOR POTENTIALS

We consider the static quark potential for separation R which is defined as $V(R)$ in lattice units. Then the color fields associated with this pair of static quarks can be measured using plaquettes of appropriate orientation. Sum rules have been derived to relate the sum over all spatial positions of these color fields to $V(R)$ and its derivative [5]:

$$\frac{-1}{b}\left(V+R\frac{\partial V}{\partial R}\right)+S_0=-\sum\ (\mathcal{E}_L+2\mathcal{E}_T+2\mathcal{B}_T+\mathcal{B}_L),$$
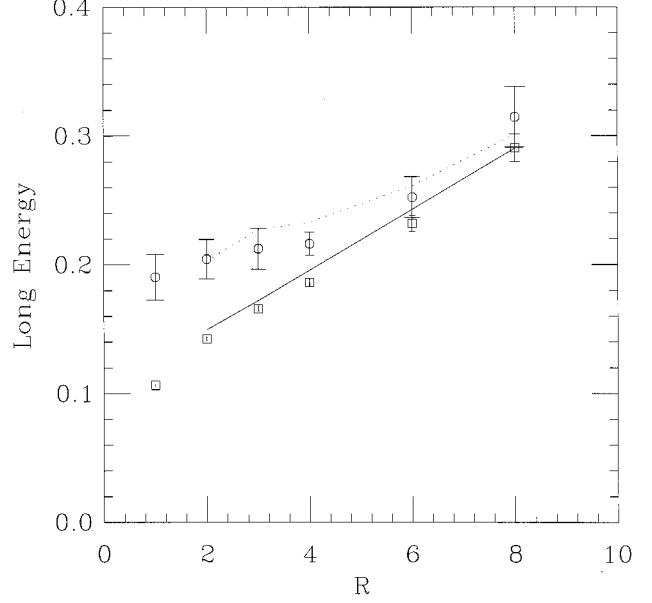$$(12)$$

FIG. 4. The color flux contributions in lattice units for separation R corresponding to the longitudinal (E_L) sum rules of Eq. (13) for the static quark potential. The expressions for the left-hand sides derived from the measured potentials are shown by the lines. The data points with $T=3$ are for the symmetric ground state (A_{1g} representation — squares) and first gluonic excitation (E_u representation — octagons).

$$\frac{1}{4\beta f}\left(V+R\frac{\partial V}{\partial R}\right)+E_0=\sum\ (-\mathcal{E}_L+\mathcal{B}_L),\qquad(13)$$

$$\frac{1}{4\beta f}\left(V-R\frac{\partial V}{\partial R}\right)+E_0=\sum\ (-\mathcal{E}_T+\mathcal{B}_T).\qquad(14)$$

Here the sum is over all space. The quantities on the right-hand sides are defined by taking correlations of appropriate plaquettes with the generalized Wilson loops as discussed in the Introduction. Because the combination $-\mathcal{E}\pm\mathcal{B}$ corresponds to energy/action, we refer to these sum rules as ''action,'' ''longitudinal energy,'' and ''transverse energy,'' respectively.

The conventional β function is defined as $b=d\beta/d\ln a$ with $\beta=4/g^2$, where g^2 is the bare lattice coupling. By considering a lattice with different lattice spacings in different directions, it is possible to define generalized β functions. At the symmetry point where $a_i=a$, one such combination is independent and is given by $U-S=\partial\beta_s/\partial\ln a_t-\partial\beta_t/\partial\ln a_t=2\beta f$ in the notations of Refs. [5,13].

The sum rules were derived [5] for torelons, where there is no self-energy associated with the static quarks. For the more practical case of the interquark potential between static sources, a self-energy term must be included in each of the sum rules — as shown above by terms S_0 and E_0. This self-energy will be independent of the interquark separation R and hence can be removed exactly by considering differences of the sum rules for two different R values. Moreover, it should be independent of spatial orientation about the source and, hence, is the same for transverse and longitudinal energy as shown above. These self-energy terms arise from the contribution of each static quark line separately, thus we
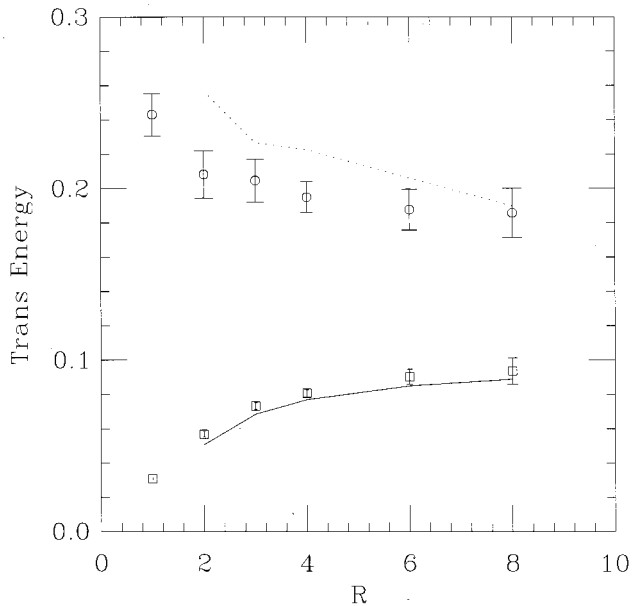
FIG. 5. The color flux contributions in lattice units for separation R corresponding to the transverse energy (E_T) sum rule of Eq. (14) for the static quark potential. The expressions for the left-hand sides derived from the measured potentials are shown by the lines. The data points with $T=3$ are for the symmetric ground state (A_{1g} representation — squares) and first gluonic excitation (E_u representation — octagons).

shall refer to both S_0 and E_0 as "self-energy" even though S_0 contributes to the action sum rule.

Our evaluations of the sum rule contribution over all space are shown in Figs. 3–5 for the symmetric (A_{1g}) and transversely excited (E_u) potentials. To isolate the contribution from the ground state in each symmetry case, we need to evaluate the color field sum using plaquettes with large separation from the operators which create and annihilate the static potential. As discussed above, using our variational operators, $T=3$ provides a reasonable approximation to this—allowing a separation of one spacing between operator and plaquette. It is important to explore the effect of any possible contamination from excited states as discussed above. The largest and, hence, best determined signal is for the action sum rule. For that case, we are able for $R \leqslant 3$ to determine the color fields for $T=4$ and 5 and our evaluations are also shown in the figures. These set the likely size of the systematic error from excited state contamination. For the A_{1g} case, the agreement with higher T values is good and confirms that we have isolated the ground state by choosing $T=3$. For the E_u case, however, such a contamination for the action sum rule could be relatively large. This is consistent with our estimates of the excited state contaminations h given above.

We now discuss the evaluation of the left-hand sides of the sum rules. One obstacle is the presence of the derivative $\partial V/\partial R$. Since only discrete values of R are measured, one way forward [8] is to eliminate this derivative between the three sum rules which still allows the generalized β functions b and f to be determined. Here we study the sum rules in a more comprehensive way by explicitly estimating the derivative. From our lattice data for the static potentials, we can find good interpolations (valid for $1 < R \leqslant 8$):

$$V(R)_{A1g} = 0.562 + 0.0696R - 0.255/R - 0.045/R^2, \quad (15)$$

$$V(R)_{Eu} - V(R)_{A1g} = \pi/R - 4.24/R^2 + 3.983/R^4. \quad (16)$$

These interpolations are illustrated in Fig. 2. Here we have used the fact that the self-energy is the same for excited and ground states, and the string model expectation that the excited state has an energy excitation of π/R for large R. The coefficients of R^{-2} and R^{-4} in these expressions are not intended to have explicit physical interpretation — we just require expressions to interpolate accurately in R.

From these expressions, we can evaluate the left-hand sides of the sum rules and they are compared with our results at $\beta=2.4$ for the color flux sum over all space in Figs. 3–5. We use the values of the generalized β functions determined previously [8], namely $b=-0.35$ and $f=0.61$ as an illustration. After choosing values for the self-energy terms as discussed below, we find an excellent overall agreement. The small discrepancies which remain are comparable to the systematic error expected from using $T=3$ to evaluate the color sums. Indeed for the action sum rule, our evaluations with $T=4$ and 5 are also shown and these indicate that the estimated systematic error is large enough to accommodate agreement. The slope of the action sum rule versus R gives directly the β function b. A somewhat steeper slope than that illustrated ($b=-0.35$) would fit better — particularly if the $T=4$ data are selected. A preferred value for this comparison would be $b=-0.33$. This is compatible with our determination of Ref. [8] which quoted $b=-0.35(2)$.

The perturbative expressions for these quantities in terms of the bare lattice coupling $\alpha=g^2/4\pi=1/\pi\beta$ for SU(2) color fields are [13]

$$b=-0.3715(1+0.49\alpha+\cdots), \quad f=1-1.13\alpha+\cdots. \quad (17)$$

The bare value of α is 0.13, which gives next to leading order perturbative values of $b=-0.395$ and $f=0.85$. The effective coupling is expected to be approximately twice as big which will decrease the perturbative estimate for f from 0.85 to ≈ 0.71 and improve the agreement with our nonperturbative result. For b, however, such an increase in α will make the agreement even worse by reducing b from -0.395 to ≈ -0.42. Thus a perturbative evaluation of b is unreliable.

The β function has also been studied nonperturbatively on a lattice by matching the measured potentials at two β values. Between $\beta=2.4$ and 2.5, this gave [9] $b=-0.277(4)$ and, in Ref. [14], using five values of β in the range 2.35–2.55 resulted in $b=-0.304(5)$. The value determined here is the derivative at $\beta=2.4$ rather than coming from a finite difference. The qualitative features of the two approaches are in agreement, however. A nonperturbative study of scaling [15] from a thermodynamic approach gave values of $b=-0.30$ and $f=0.66$ at $\beta=2.4$, although systematic errors are not easy to quantify since an ansatz for the functional dependence was assumed.

The simplest assumption for the self-energy contributions is that they are given by evaluating the left-hand sides, interpreting $V(R)$ as $V(R)-V_0$ with $V_0=0.562$. We find that this is a reasonable approximation for the action sum rule since,
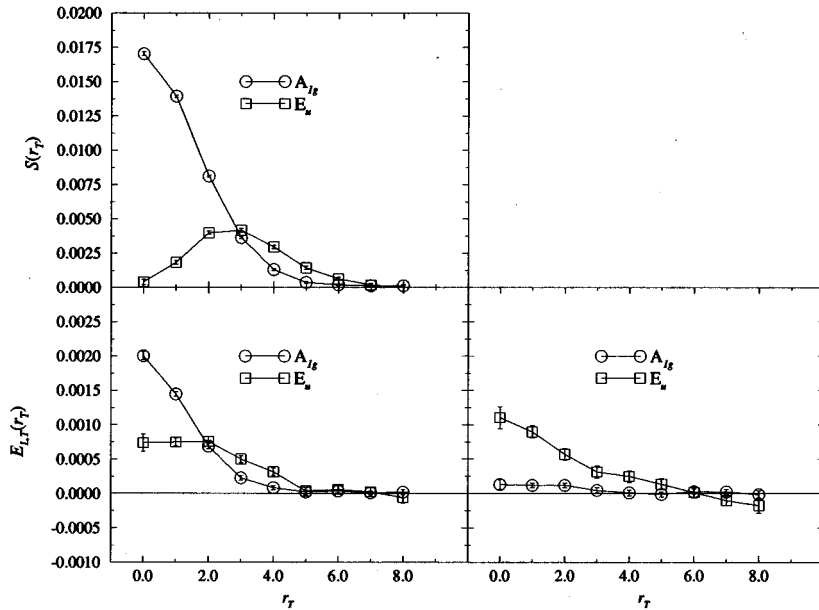
FIG. 6. The color flux contributions corresponding to the action (S), longitudinal (E_L, left plot), and transverse energy ($2E_T$, right plot) sum rules of Eqs. (12)–(14) for the static quark potential. These are shown in lattice units (with $a \approx 0.6$ GeV^{-1}) versus transverse distance r_T at the midpoint ($r_L = R/2$) for separation $R = 8$. The data are for the symmetric ground state (A_{1g} representation) and first gluonic excitation (E_u representation).

with this assumption, we have $S_0 = 0$ which is the value used in plotting Fig. 3. Using the same assumption for the two energy sum rules, however, we find that an explicit self-energy term $E_0 = 0.10$ must be used to obtain the agreement shown in Figs. 4 and 5. This self-energy should be the same for longitudinal and transverse sum rules and we find agreement with a common expression. A nonzero value arises naturally in the derivation [3] of these sum rules.

The satisfactory agreement between the sum over plaquette correlations and the sum rule expressions gives confidence that we are able to measure the color field around a static quark and antiquark. This opens up a study of the shape of the color field distribution itself.

V. COLOR FIELD DISTRIBUTIONS

Since we have measured the plaquette expectation values in the gluonic excited state (E_u), we can explore the spatial distribution of the color field and make comparison with models for the gluonic excitation such as string and flux-tube models. This has been undertaken for the ground state (A_{1g}) previously [1,2]. Comparison with models is most appropriate at large R where stringlike behavior is expected. Here we are able to reach $R = 8$ which corresponds to a separation of order 1 fm. Unfortunately, for the E_u symmetry state, the contamination from excited states (here we mean higher energy E_u representation states) is significant—being of order 30% (see Table II). As an exploratory study, we report our results using $T = 3$ for the generalized Wilson loop, since this is the largest T value with a reasonable signal. The color field distributions may then be interpreted as applying to a state which is predominantly the required lowest energy E_u state, but with some contamination from excited states.

The full spatial distribution of different components of electric and magnetic fields is a considerable body of data. Because we find that all components are approximately equal, we evaluate the combinations of color fields corresponding to the average (the action) and to those differences given by the longitudinal and transverse energy. These three combinations are also appropriate for sum rule study because they correspond to the three sum rules of Eqs. (12)–(14). To get at the essential behavior, we specialize to the midpoint ($r_L = R/2$) to minimize the effect of self-energy components. Results for the transverse dependence of the color fluxes for the action (S), longitudinal and transverse energies ($E_{L,T}$) at $R = 8$ are shown in Fig. 6 where the first excited state (E_u) case is compared with the symmetric (A_{1g}) potential case. A qualitatively similar behavior was found for $R = 6$.

We have also measured the longitudinal dependence of the sum over r_T which is illustrated in Figs. 7 and 8. Here the effect of the self-energy contributions near the sources at $r_L = 4$ units from the center can be clearly seen for the combinations corresponding to longitudinal and transverse energy.

The interpretation of these results is facilitated by the sum rules. Although the sum rules relate the sum of the color field fluctuation over all space, for a stringlike model the longitudinal dependence will be rather mild. The longitudinal profiles given by the contributions to the overall spatial sum from each longitudinal slice (fixed r_L and summed over r_T) show a fairly flat distribution in r_L for the action sum between the static sources with the E_u case showing a slightly more spread out distribution than the A_{1g} case. A similar behavior is shown by the energy sums after subtracting self-energy components. Thus some intuition can be gained about the color field sums over transverse space at the midpoint $r_L = R/2$ from looking at the left-hand sides of the sum rules divided by R.

Consider an interquark potential given by $V(R) = e/R + KR + V_0$, where the coefficient $e \approx -0.25$ for the A_{1g} potential (this is the ''Coulomb'' coefficient) while in string models we expect $e = \pi$ for the first excited string mode (which corresponds [10] to the E_u case). Then the ''transverse energy'' sum rule [Eq. (14)] will relate the sum over transverse energy fluctuations to e/R. This is consistent with the much larger transverse energy seen for the excited gluonic case (Fig. 8) compared to the symmetric ground state
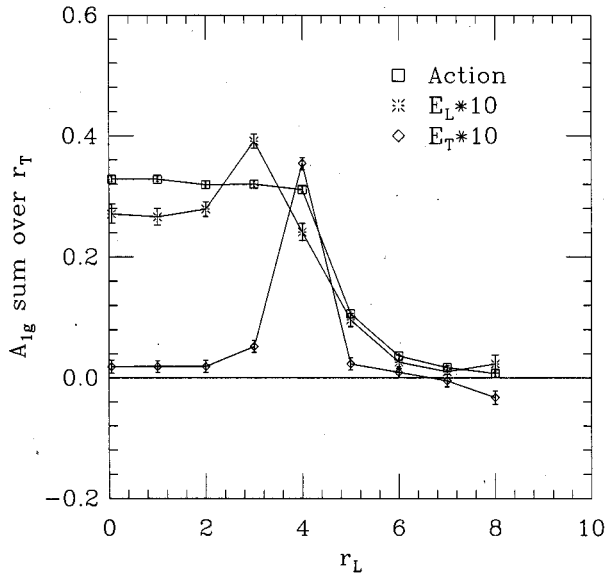
FIG. 7. The dependence on longitudinal position (r_L) of the sum over the transverse plane of the color flux contributions corresponding to the action, longitudinal (E_L) and transverse energy (E_T) sum rules of Eqs. (12)–(14) for the static quark potential. Here r_L is measured from the midpoint for separation $R=8$. The data are in lattice units for the symmetric ground state (A_{1g} representation).

potential (Fig. 7). The other two sum rules suggest that the action and longitudinal energy will have fairly similar contributions (at $r_L=R/2$ when summed over r_T) for the excited gluonic and ground state, since the left-hand side is proportional to $2KR$ in each case. We do find approximately this behavior for the integrals over r_T as shown in Figs. 7 and 8, although, as shown in Fig. 6, we see a flatter r_T distribution for the E_u case than the A_{1g} case. This flatter distribution in r_T for the excited gluonic case corresponds to a ''fatter'' flux tube for that case.

Before analyzing in detail the distributions shown in Fig. 6, we need to estimate the size of any self-energy contamination. Since $R=8$, the self-energy contributions at $r_L=4$ units from the sources are appropriate and these can be estimated from the measured plaquette correlation at 4 units from either source in the direction away from the other source. These are illustrated from our data at $R=8$ in Figs. 7 and 8 as the points with $r_L=8$. The self-energy contributions
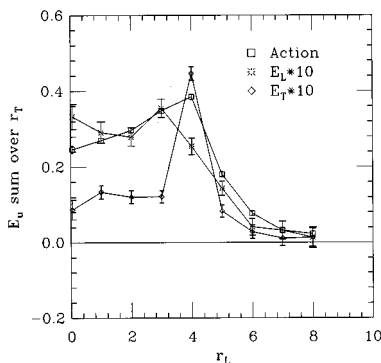

FIG. 8. As in Fig. 7, but for the first gluonic excitation (E_u representation).

here are clearly very small but, in this case, finite size effects are potentially important since the spatial length of the lattice is only 16 units. Using instead our data for the electric and magnetic color field contribution with $R=2$, 4, and 6, we find that this self-energy contribution to the measured plaquette correlation summed over r_T is less than 5% of the signal at the midpoint for $R=8$. This implies that the self-energy contribution to the action distribution is small, but that the energy distributions, which involve strong cancellations between electric and magnetic plaquettes could have larger self-energy contaminations. This self-energy contribution is large enough (and has the correct sign) to explain why the transverse energy for the A_{1g} case is positive in Fig. 6 (which contains the self-energy component) whereas the sum rule analysis described above suggests a small negative contribution (since $e<0$).

A way to eliminate the self-energy contribution completely is to focus on the difference of the A_{1g} and E_u distributions, since the distributions of the self-energy will be identical. Viewing Fig. 6 in this light, there is seen to be a significant difference in the distribution in r_T between the excited gluonic state and the ground state and it is of interest to compare this with models—the topic of the next section.

VI. MODELS FOR FLUX TUBE PROFILES

A. The model of Isgur and Paton

A bosonic quantized string will not be consistent in two transverse dimensions. In order to render the string approach applicable, Isgur and Paton (IP) [16] proposed a flux tube model in which the string degrees of freedom are reduced by considering a string made of N equally spaced masses. This discretization of the string makes the string self-energy finite and this model then makes specific predictions although they do depend in detail on N. The salient feature of the model is that the excitations are transverse and so should be observable in the transverse energy. This, indeed, is qualitatively in accord with our results, since only the transverse energy sum is greatly modified in comparing the E_u state to the A_{1g} state. Furthermore, this is also seen directly from the plot of the transverse energy profile ($2E_T$) for the Monte Carlo (MC) calculations in Fig. 6. In the next paragraphs it will be seen to what extent this qualitative feature of the IP model compares with details of these energy profiles.

In the IP model, when the string is discretized into N masses, each a distance $a_{\mathrm{IP}}=R/(N+1)$ apart, it is convenient to express the Hamiltonian in the form

$$H(\mathrm{IP},N)=\sum_{i=1}^{N} H_i(\mathrm{IP},N)=\sum_{i=1}^{N} (T_i+V_i), \qquad (18)$$

where

$$T_i=\frac{p_{x_i}^2+p_{y_i}^2}{2m} \qquad (19)$$

and

$$V_{i\neq 1,N}=\frac{b_{\mathrm{IP}}(N+1)}{2R}\frac{1}{2}[(x_i-x_{i-1})^2+(x_i-x_{i+1})^2+y's], \qquad (20)$$

$$V_{i=1,N} = \frac{b_{IP}(N+1)}{2R}\left[x_i^2 + \frac{1}{2}(x_i - x_{i\pm 1})^2 + y's\right]. \quad (21)$$

Here m is the mass of each of the N points and b_{IP} is the *bare* string energy. The two are related by $m = b_{IP}a_{IP}$. In this part of the paper, for clarity, there is a notation change with the earlier r_L, r_T now becoming z_i, $\sqrt{x_i^2 + y_i^2}$.

The energy profile associated with the point z_i on the line connecting the two quarks has the form for the state $\psi_n(IP, x_1, \ldots, x_N, y_1, \ldots, y_N)$:

$$E_i^n(N, x_i, y_i, z_i) = \int \prod_{j \neq i}^N dx_j dy_j \psi^*(IP) H_i(IP, N) \psi(IP). \quad (22)$$

The energy contained in a profile for a given z_i is then

$$E_i^n(N, z_i) = \int dx_i dy_i E_i^n(N, x_i, y_i, z_i). \quad (23)$$

In most of this work $N = 3$, where for the IP ground state $(n = 1)$,

$$E_1^1(3) = E_3^1(3) = 0.3445 E_T^1 \quad \text{and} \quad E_2^1(3) = 0.3109 E_T^1$$

and for the first excited state $(n = 2)$

$$E_1^2(3) = E_3^2(3) = 0.3464 E_T^2, \quad \text{and} \quad E_2^2(3) = 0.3071 E_T^2$$

where the total energy in state n is given by $E_T^n = (na_1 + a_2 + a_3)/m$ with $a_i = 2b_{IP}\sin(i\pi/8)$ being the IP eigenfrequencies. In each case, the kinetic K_i^n and potential P_i^n energies are approximately equal, e.g.,

$$K_2^2 = 0.1762 E_T^2 \quad \text{and} \quad P_2^2 = 0.1308 E_T^2.$$

This shows that, in spite of the averaging over $2(N-1)$ coordinates (x_i, y_i), the resultant E_i^n, T_i^n, P_i^n are still very much as expected from the basic simple harmonic oscillator structure of the original $H(IP, N)$. In general,

$$\Delta E_{IP}(n' - n, N) = E_T^{n'}(N) - E_T^n(N) = (n' - n)a_1(N)/m$$

$$= (n' - n)\frac{2(N+1)}{R}\sin\left(\frac{\pi}{2(N+1)}\right)$$

$$\xrightarrow{N \to \infty} (n' - n)\pi/R. \quad (24)$$

For $N = 1, 3$ this is already a good approximation to the $N \to \infty$ limit with $\Delta E_{IP}(n' - n, N)/\Delta E_{IP}(n' - n, \infty) = 0.90, 0.97$, respectively. Another point to note is that the energy profile $E_i^n(N, x_i, y_i, z_i)$ in Eq. (22) is proportional to b_{IP}, so that, for $r_T = 0$, it can be tuned to fit the corresponding lattice result. However, the energy contained in a given profile $E_i^n(N, z_i)$ in Eq. (23) is independent of b_{IP}.

In the lattice calculation it is the energy and action densities that are measured, i.e., basically in units of GeV/fm^3, whereas the IP model gives the energy $E_i^n(N, x_i, y_i, z_i)$ distributed on a series on N planes through the points z_i, i.e., in units of GeV/fm^2. To be able to compare the two it is nec-
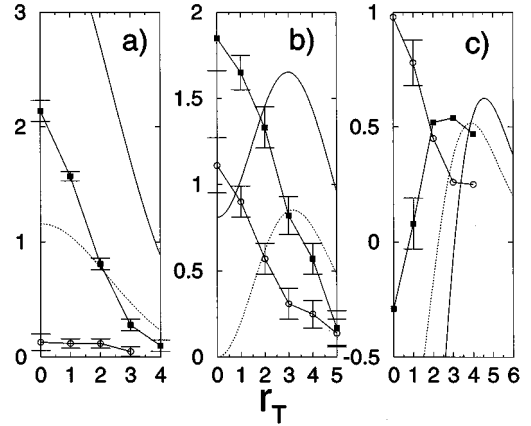

FIG. 9. The energy density at the midpoint versus transverse distance. The lattice data are at $R = 8$ (using $T = 3$) and are for the total energy (solid squares) and transverse component of the energy (open circles). The predictions of the IP model are for $N = 1, 3$ (dotted, solid). The comparison is presented in lattice units: (a) For the gluonic ground state (A_{1g}): (b) For the gluonic first excited state (E_u): (c) The differences $(E_u - A_{1g})$ between the profiles in (a) and (b). [Compared with Fig. 6 — for convenience, the profiles (in lattice units with $a \approx 0.6$ GeV^{-1}) have been multiplied by a factor of 10^3.]

essary, to smooth out the $E_i^n(N, x_i, y_i, z_i)$ into neighboring regions away from the N planes. This is most easily achieved by defining an $\bar{E}^n$ such that

$$\bar{E}^n(N, x, y, z) = \frac{E_i^n(N, x, y, z)}{a_{IP}} \quad \text{for} \quad \left(z_i - \frac{R}{2(N+1)}\right)$$

$$\leqslant z \leqslant \left(z_i + \frac{R}{2(N+1)}\right). \quad (25)$$

In the following, it is $\bar{E}^n$ that is compared with the MC results. Figure 9 shows—separately for the ground state $(n = 1)$ and first excited state $(n = 2)$ — the energy profile predictions of the IP model with $R = 8$ and $N = 1, 3$ on the plane passing through the center of the axis connecting the two quarks. This illustrates the strong N dependence referred to earlier with the $N = 3$ profiles being much larger than those for $N = 1$. But this is expected, since their $3d$ spatial integrals have the form $E_T^n = (na_1 + a_2 + a_3)/m$ for $N = 3$ and na'/m for $N = 1$, where $a_i = 2b_{IP}\sin(i\pi/8)$ and $a' = 2b_{IP}\sin(\pi/4)$. On these same figures the MC results are also plotted for the total energy and its transverse component, since the latter shows the qualitative features expected from a string-based model. But at this stage it is premature to compare the IP and MC results for a given state, since — as in the sum rule case — the two approaches involve different self-energies. Therefore, in Fig. 9(c) the profile differences between the two states are shown. However, it is seen that the IP predictions still do not correspond to the MC results. Here the value of the string energy used in the IP model has been the empirical value of $b_s a^2 = 0.07$ — but there is no reason for the bare string energy (b_{IP}) relevant to the IP model to have this same value. Unfortunately, tuning b_{IP} does not help, since the radial integrals of the IP profiles are
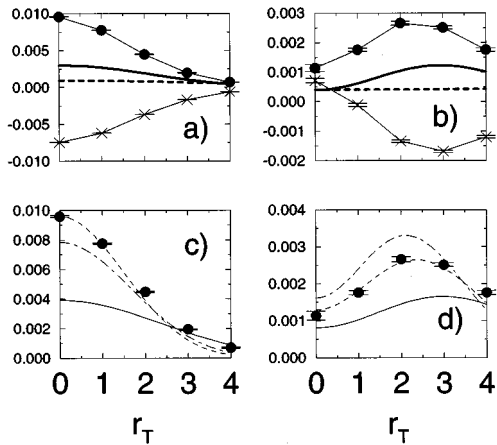
FIG. 10. Contributions to the energy density at the midpoint versus transverse distance. Comparison at $R=8$ between the $T=3$ lattice data for the color electric field (solid circles), magnetic field (crosses), and the IP predictions for the kinetic energy (solid), potential energy (dashed): (a) For the gluonic ground state (A_{1g}). (b) For the gluonic first excited state (E_u); and comparison between the color electric field $\mathcal{E}$ (solid circles) and the total energy for the IP model—using $b_{IP}=b_s=0.07$ (solid line), $b_{IP}=2b_s$ (dash-dotted), and b_{IP} tuned to fit lattice data (dashed line). (c) For the gluonic ground state (A_{1g}) tuning factor 2.45 for the dashed line. (d) For the gluonic first excited state (E_u) tuning factor 1.6 for the dashed line. All profiles are in lattice units with $a\approx 0.6$ GeV^{-1}.

constrained to be $\approx a_1/Nm$—as discussed above — and also the MC results have the similar constraints due to the sum rules in Eqs. (12)–(14). Therefore, any attempt to improve the IP model on the axis simply moves the position of the node further from the axis. The IP model is expected to be best for large values of R and is the reason for making the above comparisons at $R=8$. However, with smaller values of R, the results are still qualitatively the same with no indication that the situation has improved as R increases from 4 to 8.

Since the IP model is quite easy to use and is also, at present, the only model capable of dealing with excited states, it is of interest to try to locate a reason for its poor agreement with the MC data. Here we study the transverse profile of different components of the total energy density at the midpoint both on a lattice and in the IP model. In Figs. 10(a) and (b) we show the contributions from the electric $\mathcal{E}$ and magnetic $\mathcal{B}$ terms in Eq. (5) from the lattice and from the kinetic energy K and the potential energy P of the IP model. The self-energy contributions to these electric and magnetic contributions are expected to be small as argued above. There does not seem to be any prospect of identifying the IP model contributions to the kinetic and potential energy separately with the lattice electric and magnetic contributions (or vice versa) even invoking the freedom to set the scale in the IP model by choosing the bare string tension. The feature of the lattice data that there is a large cancellation between the electric and magnetic contributions to the energy is known to have its origin [3,4] in the trace anomaly of QCD. This is not present in a semiclassical model such as the IP model. One way to interpret these results is to note that the IP flux tube model treats the flux tube as smooth whereas the empirical lattice results show a rough color flux trajectory.
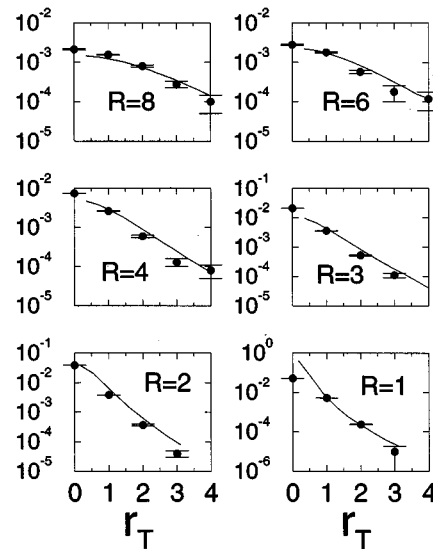

FIG. 11. On a semilog scale, a comparison of the total energy profile for the BBZ model of Ref. [18] (solid line) and the lattice predictions (solid circles) for R ranging from 8 down to 1 lattice unit. All profiles are in lattice units with $a\approx 0.6$ GeV^{-1}.

One suggestion is to interpret the energy density of the IP model as reproducing the electric color flux only [17]. In fact this is already implied in the original IP work. This can be justified if the motion of the flux tube in the model is taken to be nonrelativistic so that magnetic contributions will be suppressed. The comparison of this approach is shown in Figs. 10(c) and (d). By using the freedom to set the bare string tension in the IP model, a reasonable description of both the ground state and first excited state distributions can be achieved. Here the dash-dot curves correspond to a compromise choice of bare string tension of $2b_s$, which allows both ground state and first excited state to be described simultaneously.

B. The dual potential model of Baker, Ball, and Zachariasen

The attraction of the IP model is its extreme simplicity. However, there are other models in which flux-tube profiles can be calculated. In Ref. [18] a model proposed by Baker, Ball, and Zachariasen (BBZ), based on dual potentials, was developed that is expected to be best for large values of R. Also for technical reasons it is very difficult in this model to calculate the transverse profiles for small values of r_T without introducing large errors. Since the overall scales, in both the BBZ model and in the lattice calculations, are set by the observed string energy, it is not the absolute magnitudes that are of interest, but more the comparison between the shapes of the profiles. In Fig. 11 it is seen that the two have similar ranges and, surprisingly, the BBZ model does not seem to deteriorate significantly as R decreases from 8 to 1 lattice unit. This comparison is done more quantitatively in Table III. There the ranges of the lattice and BBZ energy profiles are fitted with the function $(A+Br_T)\exp(-Cr_T)$. For the lattice case all the available data is used in the fit, i.e., $0\leqslant r_T\leqslant 3$ or 4 lattice units. However, for the BBZ model different ranges of r_T are considered. In case I the range is approximately the same as that covered by the MC data. In II

TABLE III. Comparison between the inverse ranges (C) of the energy profiles for the lattice (MC) and the BBZ model of Ref. [18] — by fitting with the form $(A + Br_T)\exp(-Cr_T)$. The C are in units of $1/a \approx 8.3$ fm^{-1}. MC : C for the lattice data; BBZ I : C for the BBZ model over the range $0.2, 0.4 \leqslant r_T \leqslant 3.0, 4.0$; BBZ II : C for the BBZ model over the range $0.2, 0.4 \leqslant r_T \leqslant 5.0, 6.0$; BBZ III : C for the BBZ model over the range $1.0 \leqslant r_T \leqslant 3.0, 4.0$.

	R	8	6	4	3	2	1
MC		1.19(7)	1.60(13)	1.91(8)	2.19(8)	2.32(1)	3.64(5)
BBZ	I	1.05(1)	1.26(1)	1.71(9)	2.43(1)	3.50(1)	6.27(2)
	II	1.11(1)	1.26(1)	1.55(1)	2.42(1)	2.45(1)	6.27(2)
	III	1.13(2)	1.33(1)	1.61(3)	1.81(4)	2.47(1)	4.13(6)

the range is extended by about 2 lattice units and it is seen that this leads to smaller values of C for the smaller values of R. In case III — probably the most realistic — the BBZ model is restricted to $r_T \geqslant 1.0$, i.e., those values of r_T for which it can be reliably evaluated, and also r_T values upto the maximum for the lattice data. It is seen that this last case does indeed correspond quite closely to the trend shown by the lattice results.

Since the BBZ model (unlike that of IP) is not a semiclassical model and contains explicitly the trace anomaly, it may be possible to also make realistic predictions about the action. This would be of considerable interest, since the value of the action is much larger than that of the energy and so on the lattice can be extracted with greater accuracy to larger values of r_T and so serve even better in comparisons with the BBZ model.

VII. CONCLUSIONS

We evaluated sum rules for the action, longitudinal energy, and transverse energy for a range of R values. We conclude that all the sum rules at $\beta = 2.4$ are consistent with a set of generalized β functions with values of $b = -0.35(2)$ and $f = 0.61(3)$. These nonperturbative values are not in agreement with those obtained by the first two terms in the perturbative expression. An extension of our methods to larger β values would be of interest to study this discrepancy as the coupling constant is decreased.

The distribution of the color fields around a static quark and antiquark at separation R has been explored. For the symmetric ground state potential (A_{1g}), the results are in agreement with previous studies. We also determine the distribution for the lowest gluonic excitation (E_u) for the first time. For this excited state, the action distribution shows a central node in its transverse dependence. The general features of the energy distribution are an enhanced contribution in the transverse energy and a flatter distribution with r_T. These features are compared with string inspired models and with intuition from sum rules. Although no comprehensive model for the observed behavior is currently available, two positive features emerge. Firstly, the Isgur-Paton model [16] predicts an energy profile that has a very similar shape to that of the electric field squared $\mathcal{E}$ on the lattice [Figs. 10(c), (d)] and, secondly, the dual potential model of Baker, Ball, and Zachariasen [18] predicts the correct trend for the shape of the lattice energy profile even for small values of R, where their model should not be applicable (Table III).

ACKNOWLEDGMENTS

[1] G. Bali, K. Schilling, and C. Schlichter, Phys. Rev. D **51**, 5165 (1995).

[2] R.W. Haymaker, V. Singh, and Y. Peng, Phys. Rev. D **53**, 389 (1996).

[3] C. Michael, Nucl. Phys. **B280**, 13 (1987).

[4] H. Rothe, Phys. Lett. B **355**, 260 (1995).

[5] C. Michael, Phys. Rev. D **53**, 4102 (1996).

[6] I.H. Jorysz and C. Michael, Nucl. Phys. **B302**, 448 (1988).

[7] G. Bali, C. Schlichter, and K. Schilling, Phys. Lett. B **363**, 196 (1995).

[8] C. Michael, A.M. Green, and P.S. Spencer, Phys. Lett. B **386**, 269 (1996).

[9] S. Perantonis, A. Huntley, and C. Michael, Nucl. Phys. **B326**, 544 (1989).

[10] S. Perantonis and C. Michael, Nucl. Phys. **B347**, 854 (1990).

[11] UKQCD Collaboration, S. P. Booth *et al.*, Nucl. Phys. **B394**, 509 (1993).

[12] L.A. Griffiths, C. Michael, and P.E.L. Rakow, Phys. Lett. **129B**, 351 (1983).

[13] F. Karsch, Nucl. Phys. **B205**, 285 (1982).

[14] P. Pennanen, Report No. hep-lat/9608147 (unpublished).

[15] J. Engels, F. Karsch, and K. Redlich, Nucl. Phys. **B435**, 295 (1995).

[16] N. Isgur and J.E. Paton, Phys. Rev. D **31**, 2910 (1985).

[17] V.P. Nair (private communication).

[18] M. Baker, J.S. Ball, and F. Zachariasen, Phys. Rev. D **51**, 1968 (1995); Int. J. Mod. Phys. A **11**, 343 (1996); (private communication).